2+1 dimensional inversion of helioseismic travel times to infer solar flows

Jason Jackiewicz[1], **Laurent Gizon**[1], **Aaron C. Birch**[2]
[1]Max Planck Institute for Solar System Research, 37191 Katlenburg-Lindau, Germany
[2]NWRA CoRA Division, 80301 Boulder, USA

1. INTRODUCTION: INVERSION for SOLAR FLOWS

IT is well known that helioseismic travel times contain information about flows. Extracting accurate information requires a model of the effect of flows on travel times and a robust inversion procedure. Here we show results from a fully consistent procedure that are a step toward this goal. We have developed three-dimensional travel-time sensitivity kernels for vector flows in the first Born approximation (see poster PH.36), as well as a 2+1 dimensional optimally localized averaging (OLA) linear inversion scheme, explained below. The consistency lies in the fact that we measure travel times using the same definition with which the kernels are computed, as well as taking into account the full noise covariances of the travel times. We present results of inversions for near-surface flows using surface-gravity wave (f-mode) and p-mode travel times measured from full-disk MDI/SOHO Doppler data. We find that we can obtain three-dimensional maps of the vector flows at a spatial resolution as high as several megameters, and we apply this technique to image quiet-sun supergranulation as well as flow structures around an active region.

A procedure for inverting travel times for 2D flows was described in [1]. We outline this method below and its extension to include a 1D inversion in the depth coordinate to obtain the full 3D flows. The rest of this poster provides example calculations of the following recipe:

- Measure travel times for all waves that have the same radial order (mode ridge). This is done for the f, p_1, p_2, p_3, and p_4 mode ridges.
- Compute 3D kernels based on the travel-time measurements for each mode ridge, based on an accurate background solar model, that give the linear sensitivity of travel times to small-amplitude flows. Estimate the noise-covariance matrix from this model (following [2]).
- Perform a 2D OLA inversion with the depth-integrated (2D) kernels to obtain a set of inversion coefficients (weights) for each type of travel-time measurement [1]. This inversion takes the full noise properties into account.
- Obtain 1D sensitivity kernels as a function of depth by convolving the weights from the 2D inversion with the 3D kernels at each depth slice, and then integrating horizontally.
- Do the 1D depth inversion at some target depth to obtain new weights for each mode ridge, again computing accurate error estimates.
- Convolve the travel times with the 2D weights to obtain 2D flow maps for each ridge. The resulting maps give the flows averaged over the depth of the dominant mode for that ridge.
- Combine the 2D flow maps for each ridge by using the weights from the 1D inversion, to infer the flow at some targeted depth.

2. SENSITIVITY KERNELS for FLOWS

THE problem we wish to solve can be written as follows:

$$\delta\tau(\boldsymbol{x_1},\boldsymbol{x_2}) = \iiint \mathbf{K}(\boldsymbol{x_1},\boldsymbol{x_2};\boldsymbol{r})\cdot\boldsymbol{u}(\boldsymbol{r})\,\mathrm{d}^3\boldsymbol{r} + n, \qquad (1)$$

where **K** denotes the 3D sensitivity kernel, $\boldsymbol{u}$ is the small-amplitude flow perturbation, $\boldsymbol{r} = (\boldsymbol{x}, z)$ is the 3D position coordinate, and $\delta\tau$ is the wave travel-time change between the two photospheric points $\boldsymbol{x_1}$ and $\boldsymbol{x_2}$ due to the flow. The quantity n denotes noise in the travel-time measurements due to stochastic processes. We have computed kernels **K** for a realistic solar model using the Born approximation, for f modes (shown below in Fig. 1) and several p-mode ridges (see [3] and poster PH.36).

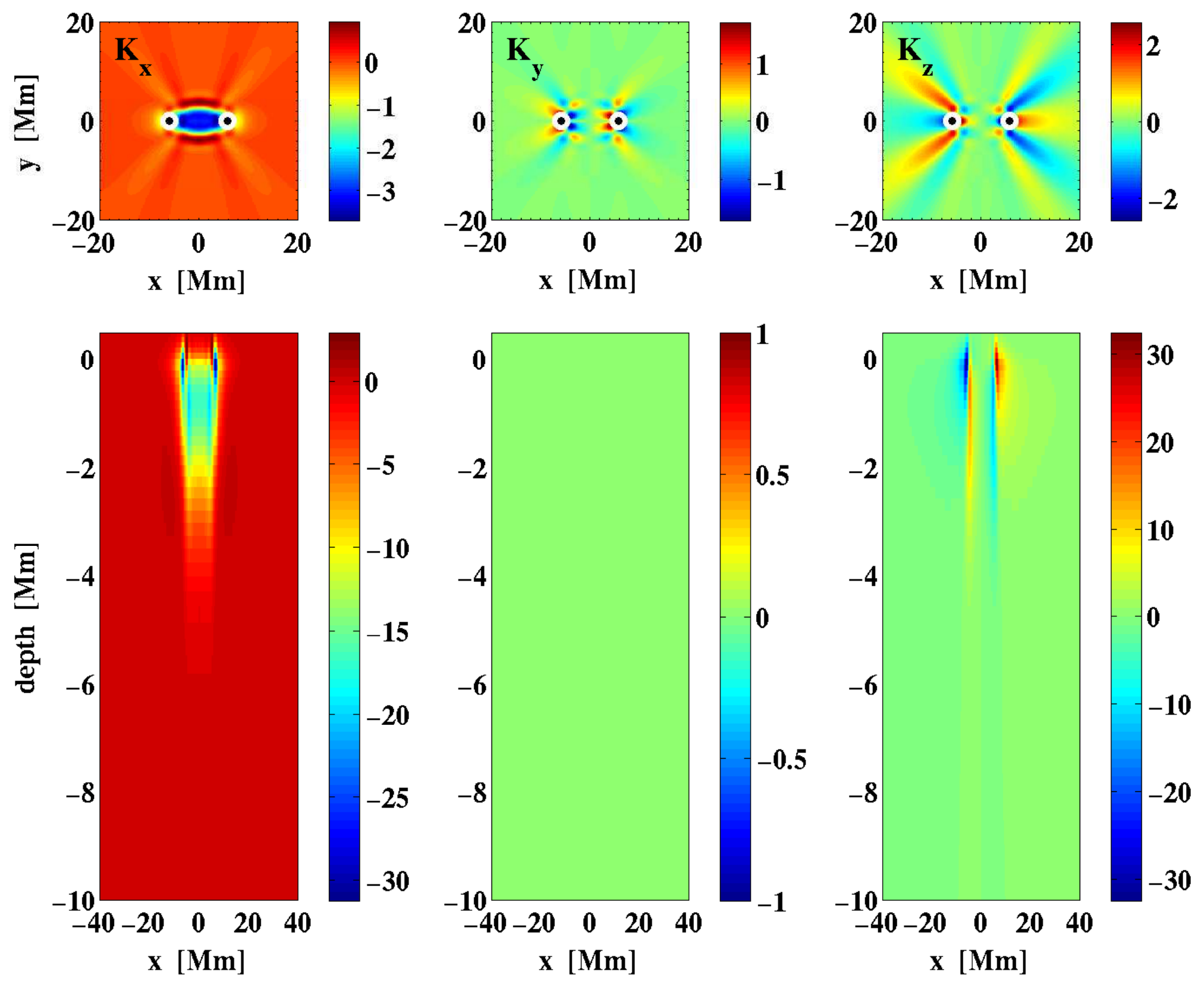

Figure 1: Surface-gravity wave (f-mode) sensitivity kernel for each component of the flow. The top panel represents a 2D kernel, obtained by a depth-integration of the full 3D kernel, slices of which along $y = 0$ are shown in the corresponding bottom panel. The 2D kernels in the top panel are the input kernels to the 2D inversion. The circles denote the observation points, which are separated by 11.68 Mm.

- In practice we use azimuthal averages of the kernel functions, to match the way the travel times are measured (point-to-annulus). This is a standard averaging procedure to reduce noise.
- For this study we use kernels for 20 different distances between the observation points, ranging from 1.5 to 30 Mm.

3. 2D HORIZONTAL INVERSION

THE OLA inversion, in essence, attempts to form a linear combination of sensitivity functions (such as those in Fig. 1) in such a way as to match a chosen target function (and at the same time not magnifying the error too much, see Sec. 5). The resulting quantity is called an averaging kernel, and the coefficients of the linear combination we will refer to as 'weights'. This allows us to solve eq. (1) for $\boldsymbol{u}$ and give a localized estimate of its value. This procedure is carried out for all 3 components of the flow separately. As an example, to invert for the component of the flow u_i, we choose the ith component of the target function to be a localized gaussian of some FWHM, at the same time choosing the target functions of the other two components to be zero. The resulting averaging kernel $\mathcal{K}_i$ is then

$$\mathcal{K}_i = \sum_\alpha w_\alpha \mathrm{K}_i^\alpha, \qquad (2)$$

where w are the weights and α in this case denotes both the type of measurement and the spatial indices. The averaging kernels for the other two components should be zero, which is desirable as to minimize the cross talk among them. Below in Fig. 2 are various averaging kernels for several different ridges and flow components. The 2D convolution implied in eq. (2) is done at each depth slice of the sensitivity kernel K_i. Note in particular from Fig. 2c that the f modes should be useful to infer vertical velocities (see Fig. 7).

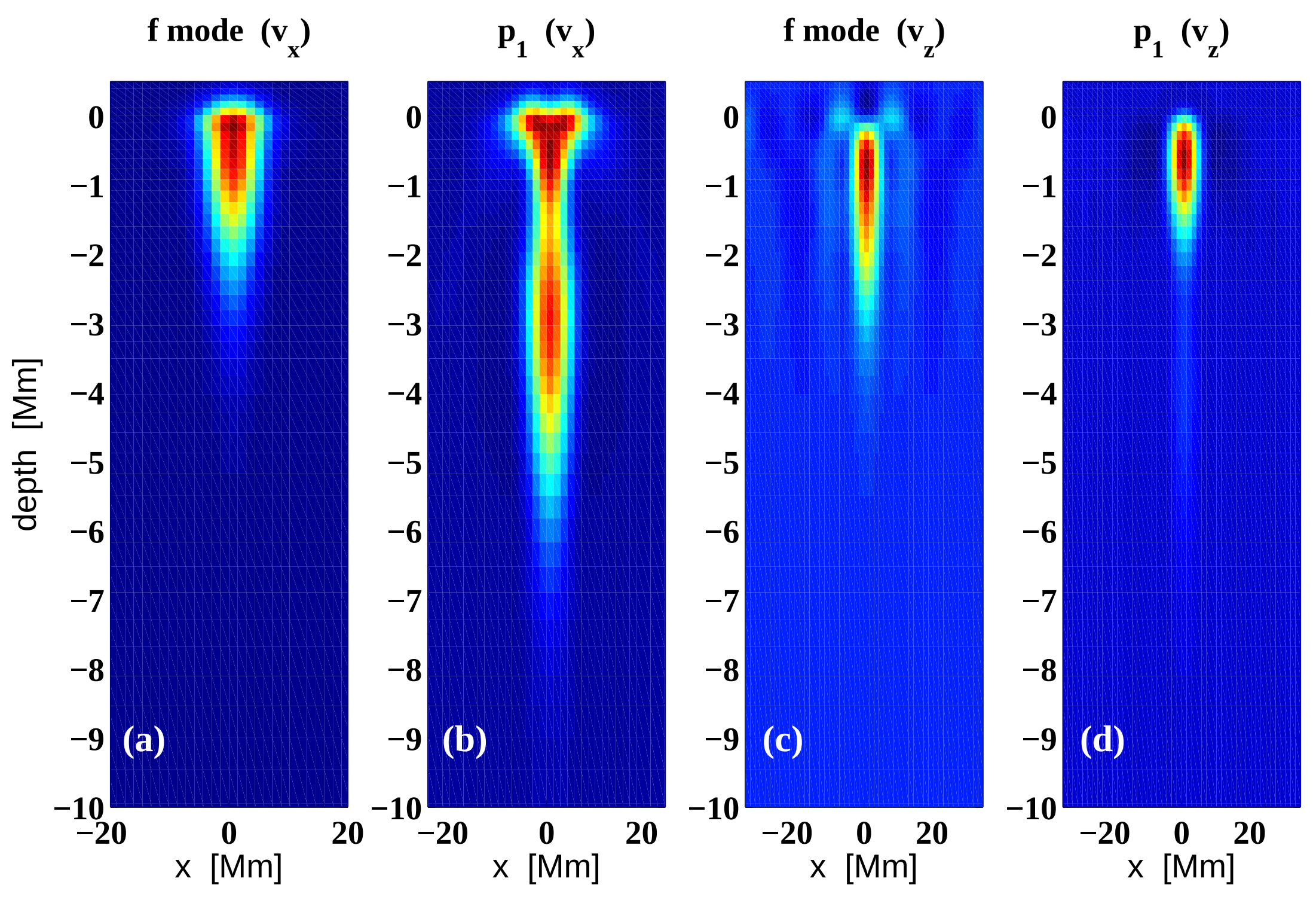

Figure 2: Depth slices along $y = 0$ of various 3D averaging kernels obtained from a 2D inversion for the flow component indicated at the top of each panel. Each inversion used a gaussian target function with a FWHM$= 7.3$ Mm.

Figure 2 shows averaging kernels for individual ridges. To obtain a more localized (in the horizontal and vertical) averaging kernel at a given depth, it is necessary to combine the averaging kernels of each ridge. To combine all of the ridges, one may imagine doing one of two things:

- Simply sum up all of the averaging kernels for each ridge, where each one is weighted by its minimum variance from the 2D inversion. This is not optimal since it does not allow any control over depth.
- Sum up all of the averaging kernels based on weights derived from 1D inversion in the depth coordinate. This will find a weighting for each ridge based on its ability to match some target function at a given depth. This will combine all of the ridges properly, and give us a way to target different depths. This is described in the next section, and will be compared to the first method.

4. 1D DEPTH INVERSION

THE 1D OLA inversion requires the same strategy as the 2D one: solve for weights $c_i(z_0)$ that combine 1D sensitivity kernels $\mathrm{K}_i^{\mathrm{1D}}(z)$ for each ridge i into a well-localized 1D averaging kernel $\mathcal{K}^{\mathrm{1D}}(z;z_0)$ about the target depth z_0. In other words,

$$\mathcal{K}^{\mathrm{1D}}(z;z_0) = \sum_i c_i(z_0)\mathrm{K}_i^{\mathrm{1D}}(z). \qquad (3)$$

The weights from the 1D depth inversion can then applied to the maps from the 2D solution according to

$$u_i(\boldsymbol{x},z_0) = \sum_i c_i(z_0)\bar{u}_i(\boldsymbol{x}), \qquad (4)$$

where the $\bar{u}_i(\boldsymbol{x})$ are the solutions to the 2D inversion problem (see Sec. 3), and $u(\boldsymbol{x}, z_0)$ are the estimated flows at a depth z_0. The 1D sensitivity functions $\mathrm{K_i}^{\mathrm{1D}}(z)$ in eq. (3) are obtained by horizontally integrating averaging kernels such as the ones in Fig. 2. These kernels are shown in the left panel of Fig. 3 for each ridge. After performing the 1D OLA inversion for various target depths (we ignore the error correlations between ridges), we obtain the 1D averaging kernels such as the ones shown in the right panel of Fig. 3.

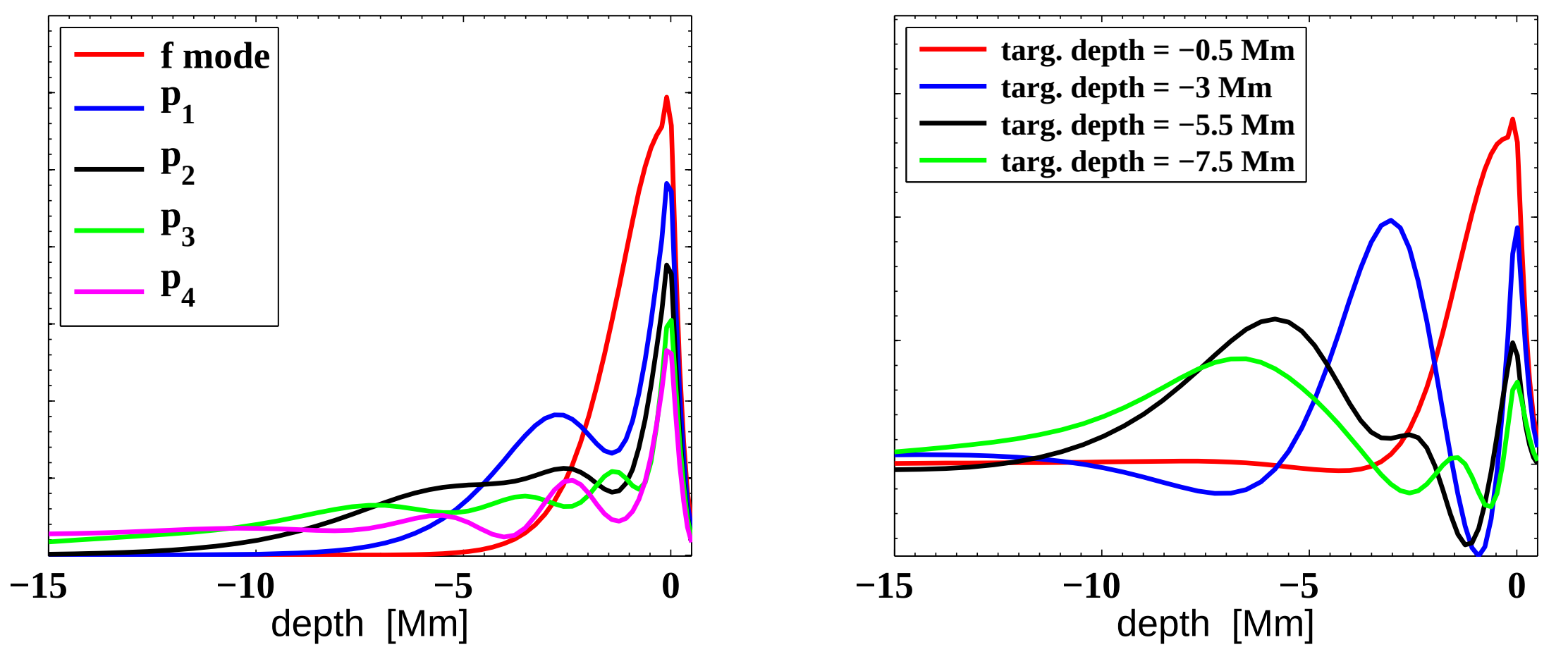

Figure 3: *Left:* 1D kernels for each ridge, obtained by horizontally integrating kernels such as the ones in Fig. 2. *Right*: Averaging kernels after the 1D inversion for various target depths.

AS can be seen from the above figure, it is difficult to get a well-localized averaging kernel for deep targets with only the 5 ridges used here. Nonetheless, the 1D depth inversion does provide a set of weights that allows us to combine the ridges in such a way as to give relatively localized averaging kernels, as shown in Fig. 4. This demonstrates why we need the 1D inversion. Figure 4a shows an averaging kernel obtained as described before, by weighting the averaging kernel of each ridge based on the minumum variance from the 2D inversion. Panel b, however, uses the weights from the 1D depth inversion to combine all the ridges, and is clearly narrower and much more localized around its target depth, which was taken to be $z_0 = -.2$ Mm beneath the surface to match the figure in (a). The ridge weights used to obtain this figure and others are given in Table 1.

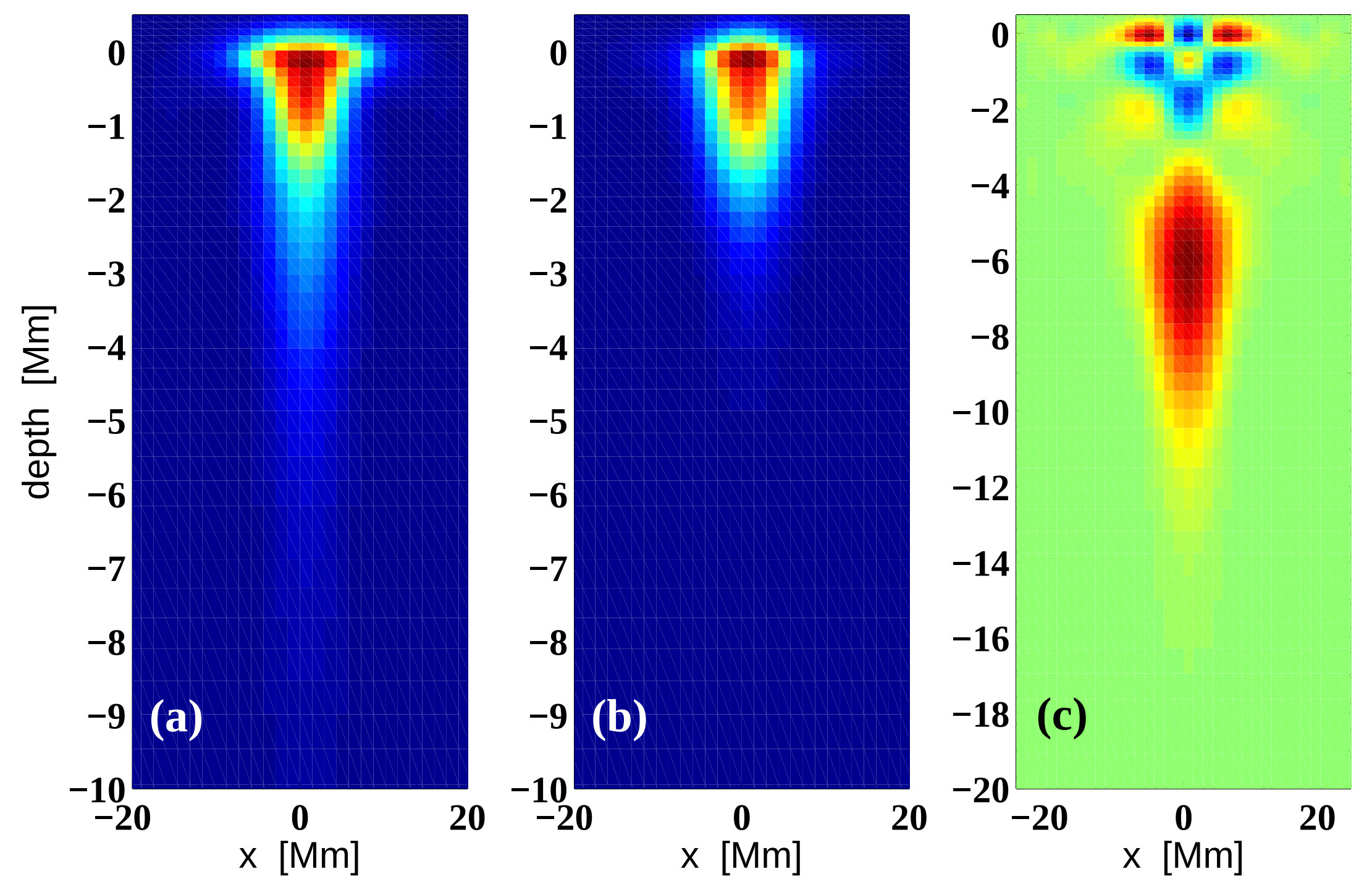

Figure 4: Averaging kernels obtained from combining the single-ridge averaging kernels. *(a)* Result from using just the minimum variance to weight each ridge. *(b)* Same input, but using weights from a 1D depth inversion for a target depth $z_0 = -0.2$ Mm. *(c)* Same as for *(b)*, but for a target depth $z_0 = -7.5$ Mm. The weights used to produce each panel are given in Table 1.

Table 1: 1D depth-inversion weights (unless otherwise noted) for each mode used to obtain the plots of Figs. 4, 5 and 6.

ridge	Fig. 4a (only errors)	Fig. 4b	Fig. 4c	Fig. 5b	Fig. 6b
f	0.62	0.97	-0.47	–	0.27
p_1	0.26	-0.07	-1.17	1.56	–
p_2	0.1	0.05	2.81	-0.59	0.75
p_3	0.02	-0.02	-0.8	0.03	-0.02
p_4	0.002	-0.01	-0.01	-0.03	-0.001

5. NOISE ESTIMATES

We are able to estimate the errors in the travel times due to random noise and the subsequent propagation of these errors through the inversion (see [1] and [2]). Here we provide these estimates for all of the relevant figures shown in this study.

Table 2: Error estimates for the figures indicated. The numbers represent the 1σ values.

Figure	Error	Figure	Error
Fig. 2a	27 m/s	Fig. 5b	70 m/s
Fig. 2b	44 m/s	Fig. 6a	42 m/s
Fig. 2c	120 m/s	Fig. 6b	48 m/s
Fig. 2d	88 m/s	Fig. 7	120 m/s
Fig. 4a	24 m/s	Fig. 8b	17 m/s
Fig. 4b	13 m/s	Fig. 9	12 s^{-1}
Fig. 4c	70 m/s	Fig. 10	13 s^{-1}
Fig. 5a	25 m/s	Fig. 14 (all panels)	21 m/s

HELAS II: Helioseismology, Asteroseismology, and MHD Connections. 20-24 August 2007, Göttingen, Germany.

6. RESULTS: MAPS of FLOWS

IN this section we show various maps of flows retrieved using the inversion procedure described above. In all cases the maps were obtained by inverting travel times measured from MDI full-disk Dopplergrams, and represent 24-hour averages. Also, in each case the set of inversion results for each skip distance ($1.5 - 20$ Mm) is averaged by using the noise correlation information. The estimated errors for all of the maps are given in Table 2.

WE first perform a very important consistency check. This is done by producing a map from an inversion using only one ridge, a 'target map'. Then we compare this to a map done with an inversion that targets the lone ridge but uses all of the other available ridges. The results are quite encouraging, and are shown in the next two figures.

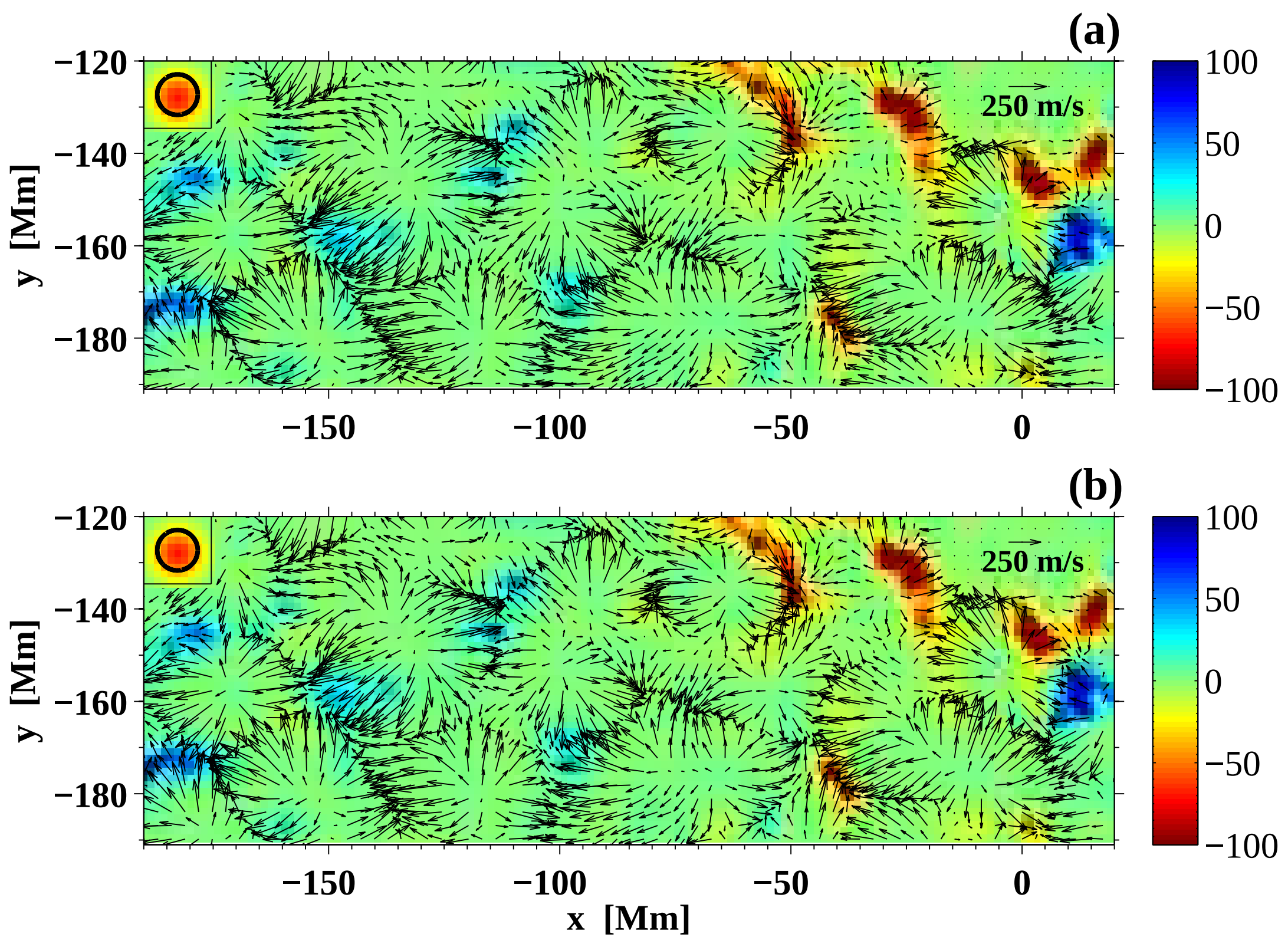

Figure 5: Quiet-sun flow maps obtained from inverting a 24 hr set of travel times. *(a)* Result from a 2+1D inversion using only f modes (the target map). *(b)* Same region of the Sun, but using only acoustic modes (p_1 to p_4 ridges) by targeting the f-mode kernel (red line of Fig. 3) in the 1D inversion. The corresponding weights are given in Table 1. The box in the top left represents the 2D gaussian target function from the 2D inversion and the circle outlines its FWHM ($= 7.3$ Mm), which is a measure of the resolution of the inversion. The color scale represents the 1 day averaged magnetic field measured in gauss and has been truncated. The correlation coefficient between these two maps is 0.99.

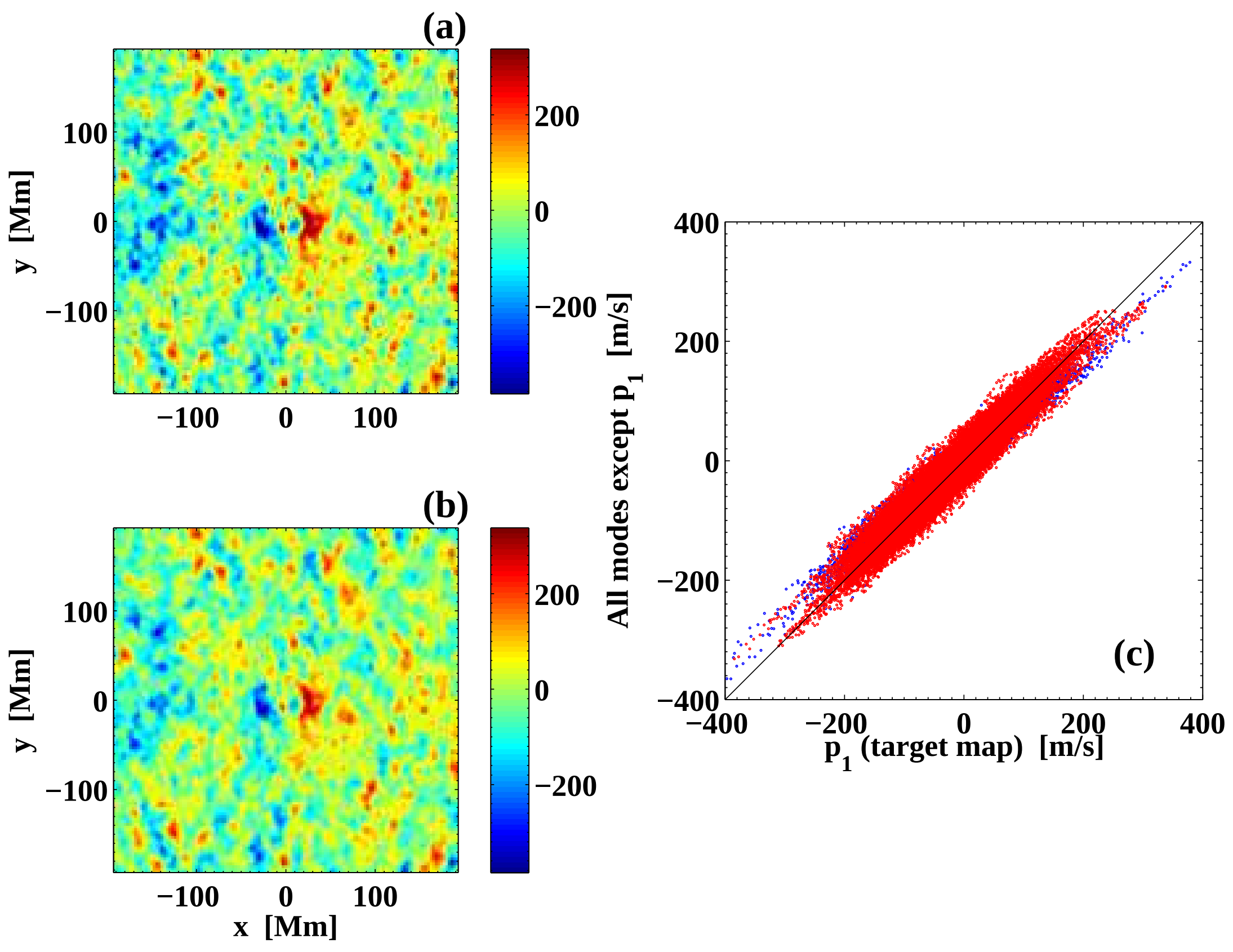

Figure 6: Similar to Fig. 5, but using p_1 as the target ridge. We also show a much larger region of the Sun, and we only plot the x component of the inferred flow. There is a sunspot in the middle of the image. *(a)* The p_1 ridge target map. *(b)* The map from combining f, p_2, p_3, and p_4. The corresponding weights are given in Table 1. *(c)* Scatterplot of the values from *(a)* and *(b)*. The red denotes pixels in the maps where the magnetic field is below 20 gauss, and the blue points for pixels above this value. The correlation coefficient between the two maps is 0.97.

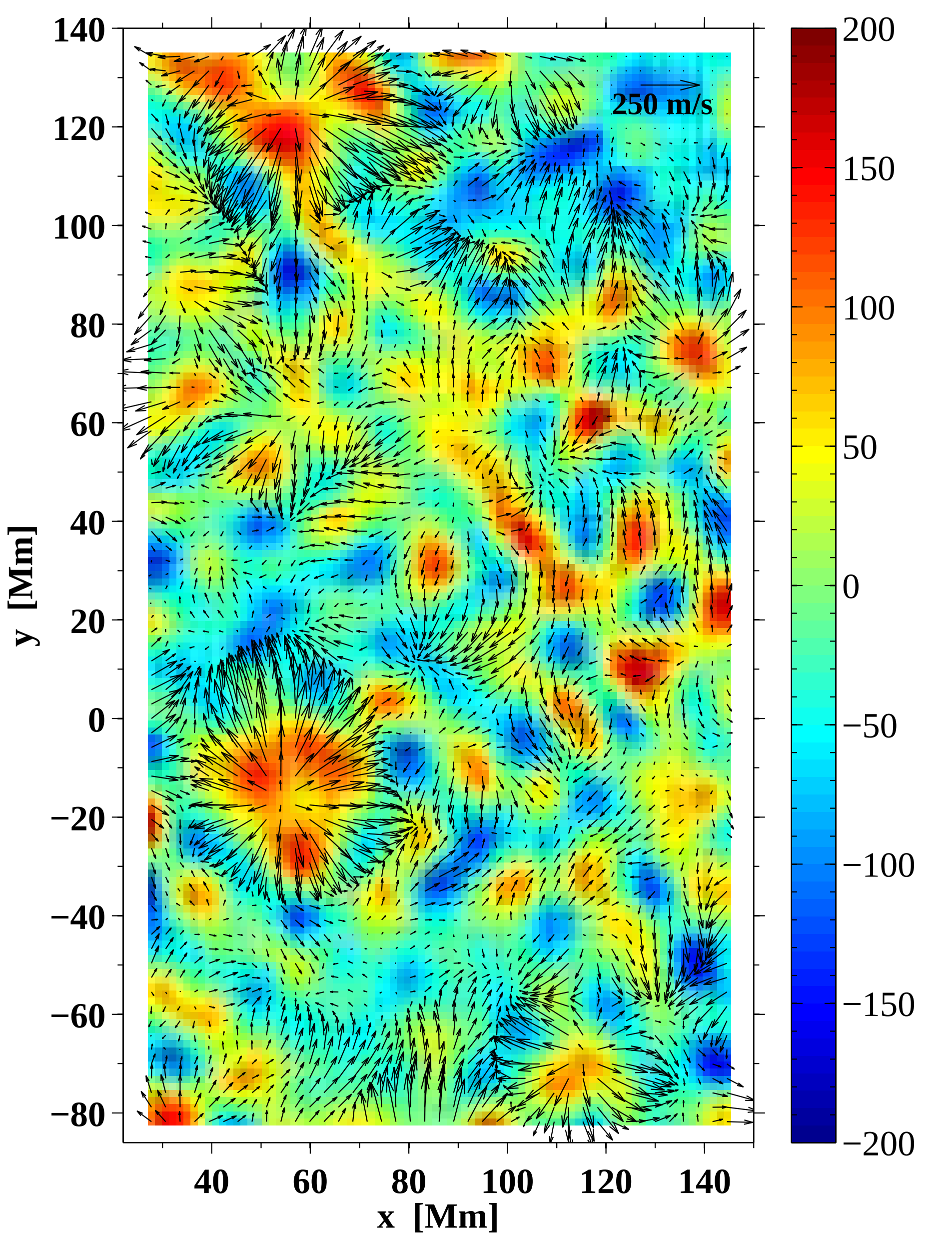

Figure 7: Horizontal flows (arrows) and vertical flows (denoted by the colormap) from an inversion using only f modes and 24 hr of data. The units of the colorbar are m s^{-1}. The target function was of a FWHM$= 7.3$ Mm. There seems to be good correlation between upflows and outflows, and downflows and inflows.

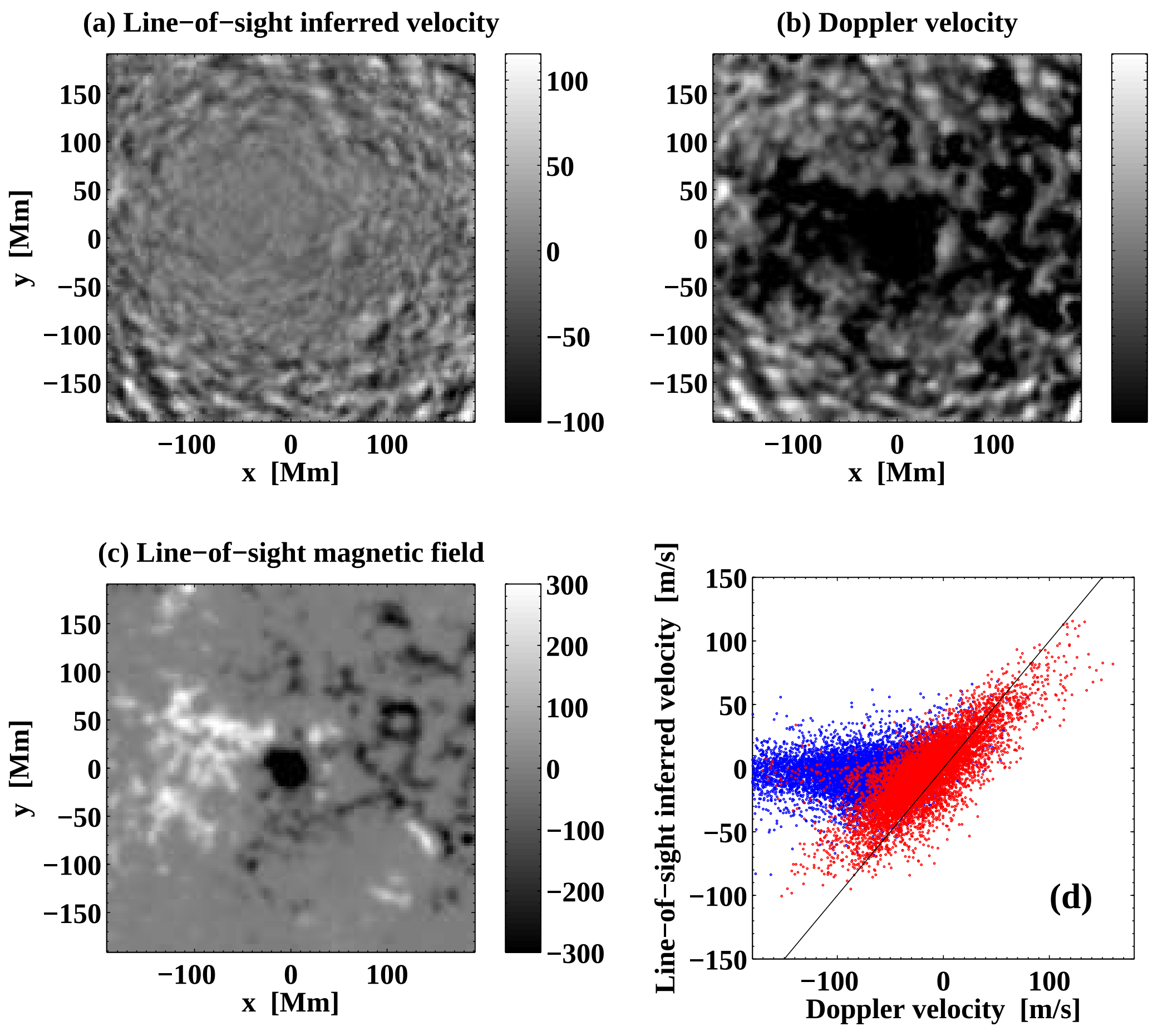

Figure 8: *(a)* Inferred velocities from an inversion using the f and p_1 ridge obtained by projecting the two horizontal components of the velocity onto the line-of-sight vector for every pixel. The inversion had a target function of FWHM$= 7.3$ Mm. *(b)* 24 hour-average Dopplergram, convolved with the same target function. *(c)* 24-hour average magnetic field for the same region, which shows clearly the big sunspot and the surrounding plage. *(d)* Scatterplot of the inferred line-of-sight velocity vs. the observed line-of-sight velocity for each pixel. Red (blue) dots represent pixels of less (more) than 15 gauss. The correlation coefficient is 0.76. The black line is a $y = x$ line to guide the eye. Note that the z component of the inferred velocities was not used in computing the projected line-of-sight values.

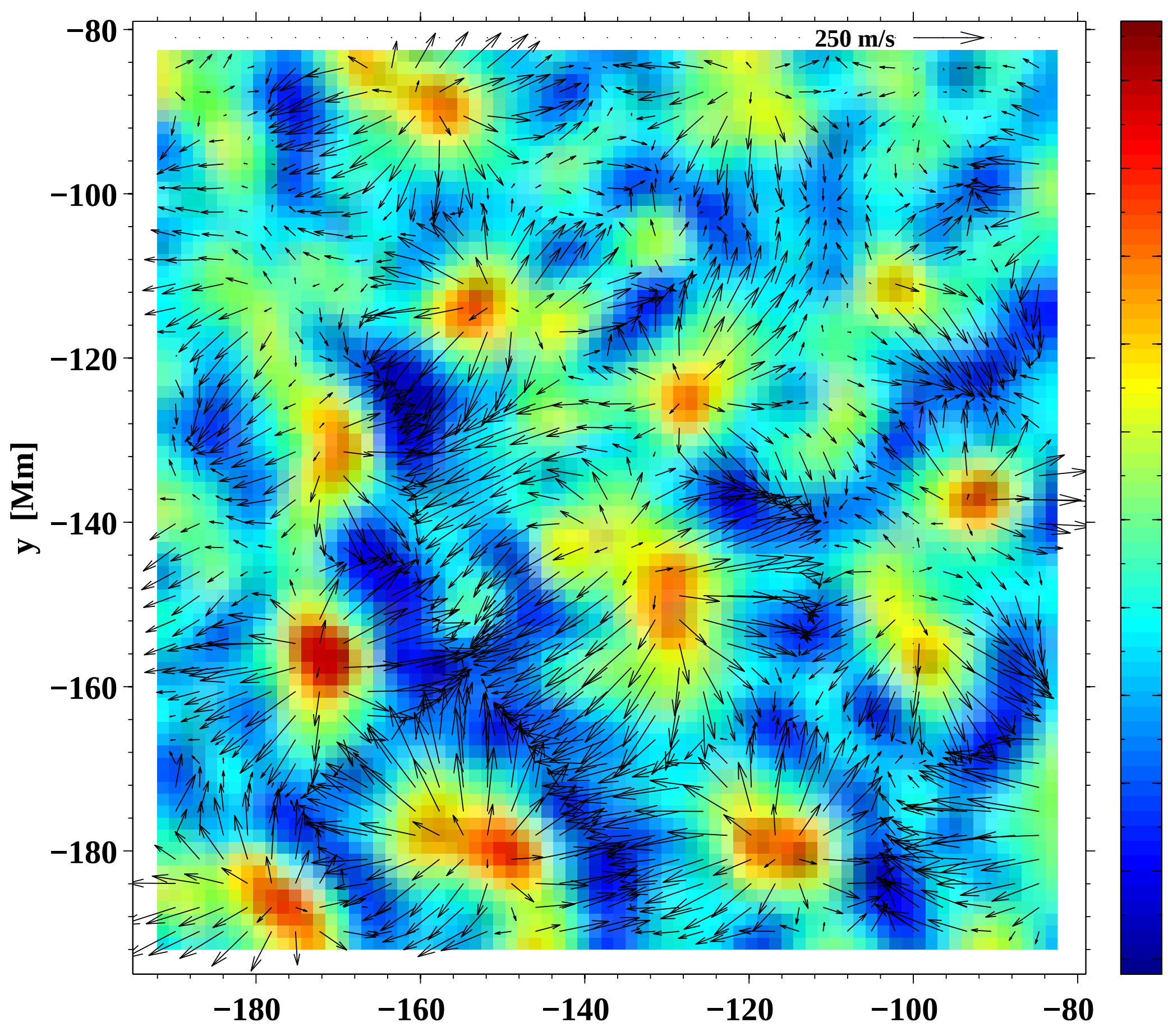

Figure 9: Flow divergence and horizontal flows from two separate 2D f-mode inversions using 24 hr of data. The arrows represent the horizontal flows, and the colors represent the flow divergence. The divergence inversion is carried out simply by using a different target averaging kernel, chosen such that the outcome of the inversion is directly the horizontal divergence. This method allows us to estimate a proper resolution of the inversion, which is not possible by simply computing the numerical divergence of the horizontal flows. The target used here had a FWHM=7.3 Mm. The units of the colorbar are s^{-1}.

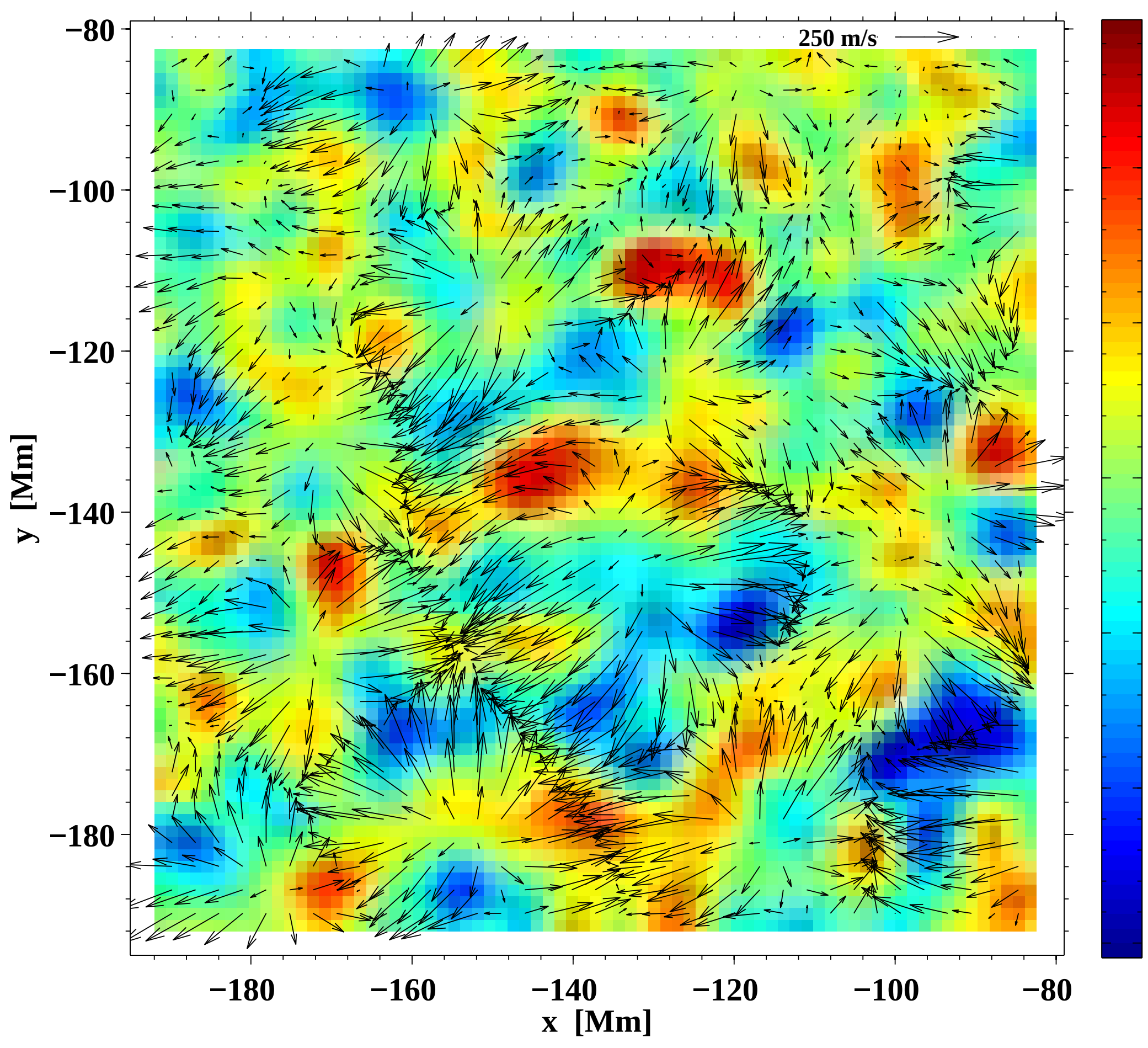

Figure 10: The vertical component of the vorticity and the horizontal flows from two separate 2D f-mode inversions using 24 hr of data. The vorticity is the result of a 2D inversion whose target averaging kernel is properly chosen. The target used here had a FWHM=7.3 Mm. The units of the colorbar are s^{-1}.

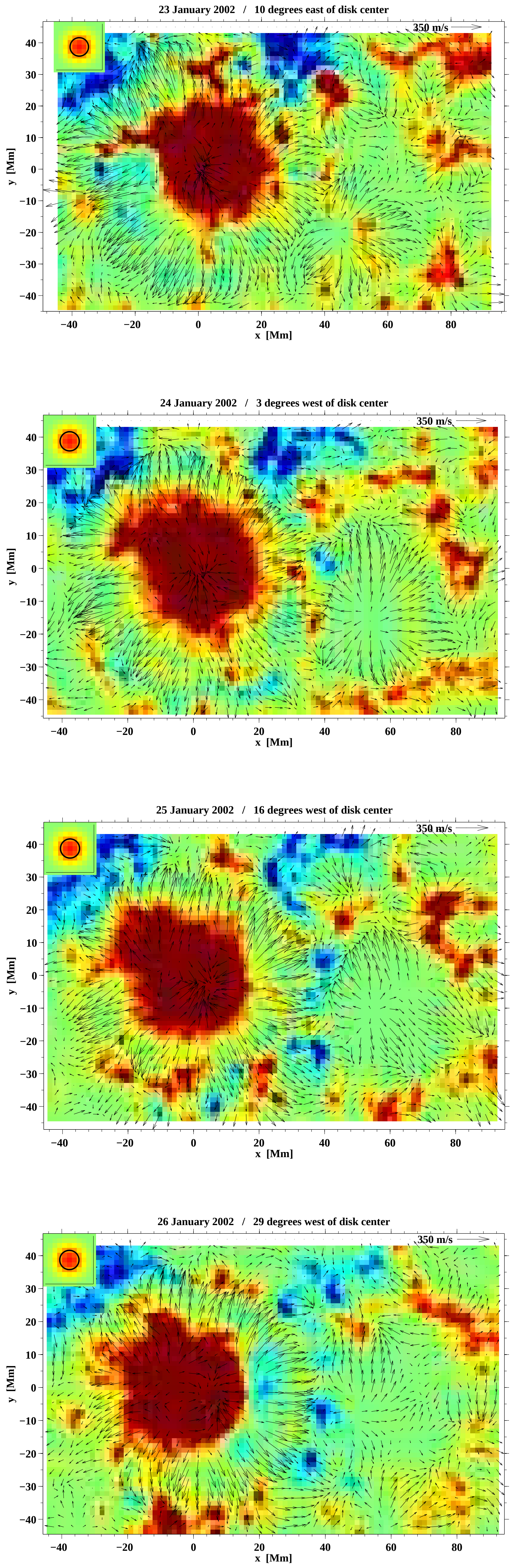

Figure 14: Evolution of flows. The above 4 figures are each 24-hour flow maps obtained from a full 2+1D inversion using all of the mode ridges available, targeting a depth of 0.5 Mm below the solar surface. The day and the longitude of the center of the umbra of the large sunspot is indicated in each panel. The latitude is a few degrees below the equator. This is active region AR9787 (see poster PH.44). The averaging kernel (resolution) is shown in the upper left corner. The color denotes the truncated (at ± 300 G) line-of-sight magnetic field averaged over the corresponding day.

7. CONCLUSIONS

- This inversion is capable of producing high-resolution maps to study the time-evolution and depth-dependence of three-dimensional flows.
- We have a very accurate estimate of the errors that come out of the inversion procedure.
- We can compute quantities such as the divergence and the vorticity properly simply by changing the target function, with no need to compute new kernels.

References

[1] Jackiewicz, J., Gizon, L., Birch, A. C., & Thompson, M. J. 2007, Astronomische Nachrichten, **328**, 234

[2] Gizon, L., & Birch, A. C. 2004, ApJ, **614**, 472

[3] Birch, A. C., & Gizon, L. 2007, Astronomische Nachrichten, **328**, 228

HELAS II: Helioseismology, Asteroseismology, and MHD Connections. 20-24 August 2007, Göttingen, Germany.